Optimal Torque Control of the Externally Excited Synchronous Machine

Sabin C. Carpiuc*, **, Corneliu Lazar*, Daniel I. Patrascu*, **

*Department of Automatic Control and Aplied Informatics,
Technical University "Gheorghe Asachi" of Iasi,
Str. Prof. dr. doc. Dimitrie Mangeron, 27, 700050, Iasi, Romania
(e-mail:clazar@ac.tuiasi.ro)

**Powertrain Division,
Continental Automotive Romania,
Blvd Poitiers, 6, 700671, Iasi, Romania
(e-mail:{ sabin.carpiuc, daniel.patrascu }@continental-corporation.com)

Abstract: The basic function of any type of electric machine used in automotive powertrain is to propel the automobile in motor mode or to recharge the high-voltage battery in generator mode. The torque control of electric machine in motor and generator modes, using more efficient high-voltage battery, is a goal for the automotive industry. A good choice for Electric Vehicles (EVs), due to many advantages, is the Externally Excited Synchronous Machine (EESM). In this paper, a new optimal torque control algorithm for EESMs that aims at optimum torque control in the entire operating range based on a dual-rate sampling solution is presented. In order to test the developed algorithm a dynamic model of EESM is designed based on mathematical equations. The model is validated against the data obtained on a system testbench. The simulated results obtained with the proposed control strategy are compared with the ones obtained with the classical PID approach and the results show improved performances.

Keywords: Externally Excited Synchronous Machine, electric vehicles, field oriented control, current referencer, constant torque region, constant power region, optimal control.

1. INTRODUCTION

Nowadays Hybrid Electric Vehicles (HEVs) and Electric Vehicles (EVs) have become an alternative to the conventional automobiles and electric machines tend to replace the internal combustion engine. The Externally Excited Synchronous Machine (EESM) is a good choice for the automotive industry because it possesses many advantages: high efficiency, high power density, high torque at startup, high reliability and an additional degree of freedom compared with the Permanent Magnet Synchronous Machine (PMSM) (Hagstedt et al. (2008)).

For a better understanding, the EESM can be analyzed using the rotor reference frame. The three-phase stator quantities (voltages, currents or flux linkages) can be transformed to the rotor reference frame and vice versa by using Clarke and Park transformations (Park (1929), Krause et al. (2002), Pillay and Krishnan (1988), Aller et al. (2002)). In the resulted model, the torque and the speed can be controlled in a similar way as for the direct current (DC) machine.

The torque control is the main challenge for any type of electric machine used in the automotive propulsion. There are two advanced control methods: Direct Torque and Flux Control (DTFC) and Field Oriented Control (FOC). FOC strategy is more suitable for applications like EVs and HEVs because it is better adapted to the load variation (Casadei et al. (2002)). DTFC is characterized by simplicity, without any current controller and without requiring any informations about the rotor position (Haque et al. (2003a)) and offers a fast dynamic response (Takahashi and Noguchi (1988)), but there are high current and torque ripples (Vasudevan and Arumugam (2004), Tang et al. (2002)). FOC basic idea is to control stator currents represented by a vector, in the rotor reference frame, by using the rotor electrical position. Controlling the stator currents, this control strategy reduces the torque ripples (Casadei et al. (2002)).

Up to now the EESM is controlled using FOC schemes based on the standard Proportional-Integral (PI) control law (Märgner and Hackmann (2010)). Considering the power efficiency issue, the performance of FOC in EESM drives can be improved by using advanced control methods such as optimal control. The optimal control theory is used with promising results in problems related to aerospace engineering (Anderson and Moore (1989)). The Linear Quadratic Regulator (LQR) can represent a possible solution for EESM drives. The LQR is an optimal control methodology where the state equation of the plant is linear and the cost function is quadratic (Anderson and Moore (1989), Goebel and Subbotin (2007)).

The entire control structure must be designed so as to take into account also the limitations of the computer based implementation in an Electronic Control Unit (ECU) (Malinowski and Yu (2011), Salewski and Kowalewski (2008), Monmasson et al. (2011)) and the limitations of the communication architecture used (Benzi et al. (2005)).

In this paper, a new optimal torque control architecture based on the FOC for EESMs is developed, taking into account both the constant torque and the constant power regions, and considering the variations of the machine parameters. The control solution, based on a dual-rate sampling approach, is designed to cover the entire operation range of the EESM. The LQR is used to ensure better performance and minimum energy consumption. The electric machine torque is estimated using the stator flux linkages and currents. The error between the reference and estimated torque is held at zero by a torque deviation controller. For testing the control scheme a dynamic model of a 60 kW three-phase EESM in rotor reference frame is designed. The model is then validated against data obtained on a system test bench.

The paper is organized as it follows. In section II, the EESM model is presented. Section III presents the proposed control structure, currents control strategy, the torque estimator, the torque deviation control strategy and the current referencer. The simulation results are shown and analyzed in section IV and conclusions are drawn in section V.

2. EESM MODEL

The standard configuration of a three-phase EESM stator is shown in Fig.1.a. After applying the transformation of axes, an imaginary structure results, as can be seen in Fig.1.b.

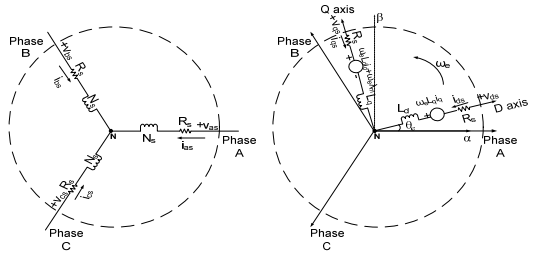

(a) (b)

Fig. 1. EESM stator structure (a) stator windings (b) 'dq' imaginary windings

From Fig. 1.a, EESM stator voltage equations are obtained by applying Kirchhoff's voltage law:

$$\begin{aligned} v_{as} &= r_s i_{as} + \frac{d\lambda_{as}}{dt} \\ v_{bs} &= r_s i_{bs} + \frac{d\lambda_{bs}}{dt} \\ v_{cs} &= r_s i_{cs} + \frac{d\lambda_{cs}}{dt} \end{aligned}, \tag{1}$$

where v_{as}, v_{bs}, v_{cs} are the three-phase stator voltages, i_{as}, i_{bs}, i_{cs} are the three-phase stator currents, λ_{as}, λ_{bs}, λ_{cs} are the three phase stator flux linkages and r_s is the stator resistance.

The rotor configuration is composed of excitation windings supplied in DC. As such, the excitation voltage equation results as:

$$v_e = r_e i_e + \frac{d\lambda_e}{dt}, \tag{2}$$

where v_e is the excitation voltage, i_e is the excitation current, λ_e is the rotor flux linkage and r_e is the rotor resistance. The rotor flux linkage is given by:

$$\lambda_e = M_d i_{ds} + L_e \cdot i_e, \tag{3}$$

where M_d is the mutual inductance between stator and rotor windings and L_e is the excitation inductance.

By applying axes transformation (Park (1929), Krause et al. (2002)), using the rotor electric position θ_e, (1) become:

$$\begin{aligned} v_{qs} &= r_s i_{qs} + \frac{d\lambda_{qs}}{dt} + \omega_e \lambda_{ds} \\ v_{ds} &= r_s i_{ds} + \frac{d\lambda_{ds}}{dt} - \omega_e \lambda_{qs} \end{aligned}, \tag{4}$$

where v_{ds}, v_{qs} are the d and q axis stator voltages, i_{ds}, i_{qs} are the d and q axis stator currents, λ_{ds}, λ_{qs} are the d and q axis stator flux linkages and ω_e is the rotor electrical angular velocity. Stator flux linkages in the rotor reference frame are expressed as:

$$\begin{aligned} \lambda_{qs} &= L_q i_{qs} \\ \lambda_{ds} &= L_d i_{ds} + M_d \cdot i_e \end{aligned}, \tag{5}$$

where L_d, L_q are the d and q axis inductances.

From the input power in view of 'dq' coordinates, the electromagnetic torque function results from (5) as:

$$T_e = \frac{3P}{4}\left[M_d i_e i_{qs} + \left(L_d - L_q\right) i_{qs} i_{ds}\right], \tag{6}$$

where P denotes the number of poles.

The equation for the machine dynamics is given by:

$$T_e - T_L = J_m \frac{d\omega_m}{dt} + B_m \omega_m, \tag{7}$$

where T_L is the load torque, J_m is the rotor moment of inertia, B_m is the viscous friction coefficient and ω_m is the mechanical angular velocity with $\omega_m = \frac{2 \cdot \omega_e}{P}$.

From the electrical angular velocity, the rotor electrical angular position is obtained as:

$$\theta_e = \int_0^t \omega_e(\zeta) d\zeta + \theta_e(0), \tag{8}$$

where ξ is the variable of integration.

3. OPTIMAL CONTROL STRUCTURE

Fig. 2 shows the proposed control structure based on a dual-rate sampling solution. The system command is given by the torque reference (T_e*).

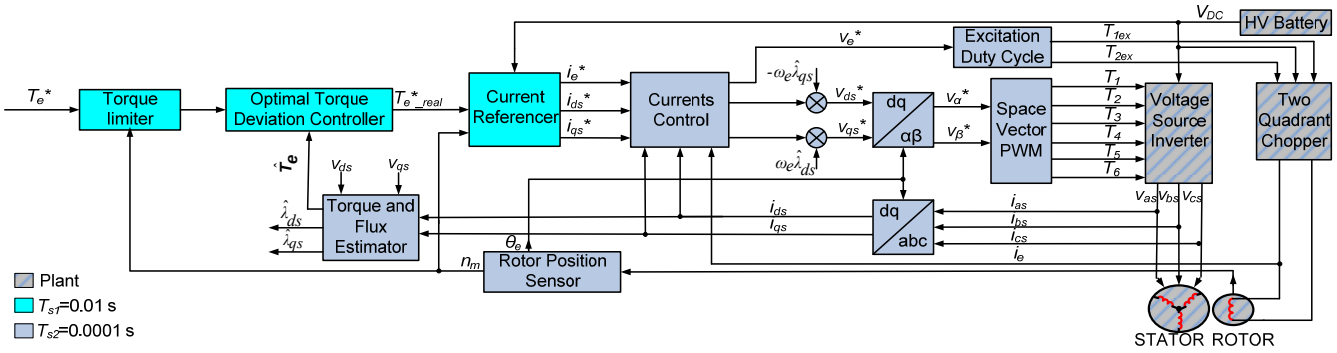

Fig. 2. EESM optimal control structure using a dual-rate sampling solution

This proposed control structure is a modified FOC structure with a torque estimator and a torque deviation controller to minimize the effect of the variation of machine parameters and to minimize looses. The current referencer generates simultaneous the stator and excitation current references in the rotor reference frame (i_{ds}*, i_{qs}* and i_e*).

The Space Vector PWM and the Excitation Duty Cycle blocks contain the modulation technique and the complex programmable logic devices (CPLD) for the generation of the power stage gate signals (T_{1e}, T_{2e} and T_1 through T_6). Modulation techniques for electronic power conversion are discussed in detail in (Holtz (1994), Kwasinski et al. (2003), Houldsworth and Grant (1984)). The Rotor Position Sensor is used to measure the rotor electrical position and speed (n_m denotes the mechanical speed in revolution per minutes). The rotor electrical position is used by axes transformations and the mechanical speed is used by the current referencer.

3.1 Currents Control

From (2) – (5) the state space model for the EESM electrical subsystem results:

$$\begin{cases} \dot{\mathbf{x}}(t) = \mathbf{A}\mathbf{x}(t) + \mathbf{B}\left[\mathbf{u}(t) + \mathbf{l}(t)\right] \\ \mathbf{y}(t) = \mathbf{C}\mathbf{x}(t) \end{cases}, \tag{9}$$

where

$$\mathbf{x}(t) = \begin{bmatrix} i_{ds}(t) \\ i_{qs}(t) \\ i_e(t) \end{bmatrix}, \quad \mathbf{u}(t) = \begin{bmatrix} u_{ds}(t) \\ u_{qs}(t) \\ u_e(t) \end{bmatrix}, \quad \mathbf{l}(t) = \begin{bmatrix} \omega_e(t)\lambda_{qs}(t) \\ -\omega_e(t)\lambda_{ds}(t) \\ 0 \end{bmatrix},$$

$$\mathbf{A} = \begin{bmatrix} \frac{L_e r_s}{M_d^2 - L_d L_e} & 0 & -\frac{M_d r_e}{M_d^2 - L_d L_e} \\ 0 & -\frac{r_s}{L_q} & 0 \\ -\frac{M_d r_s}{M_d^2 - L_d L_e} & 0 & \frac{L_d r_e}{M_d^2 - L_d L_e} \end{bmatrix},$$

$$\mathbf{B} = \begin{bmatrix} -\frac{L_e}{M_d^2 - L_d L_e} & 0 & \frac{M_d}{M_d^2 - L_d L_e} \\ 0 & \frac{1}{L_q} & 0 \\ \frac{M_d}{M_d^2 - L_d L_e} & 0 & -\frac{L_d}{M_d^2 - L_d L_e} \end{bmatrix}, \quad \mathbf{C} = \begin{bmatrix} 1 & 0 & 0 \\ 0 & 1 & 0 \\ 0 & 0 & 1 \end{bmatrix},$$

with constraints on inputs and states (currents and voltages are limited by the high voltage battery and by the electric power stage) $\mathbf{u}(t) \in U \subset \Re^3, \mathbf{x}(t) \in X \subset \Re^3$.

As it is desirable to have minimum energy consumption and zero steady state error, it is necessary to use a controller with integral actions. The proposed control algorithm for controlling the stator currents is based on the LQR. The basic principle for this control strategy is shown in Fig. 3.

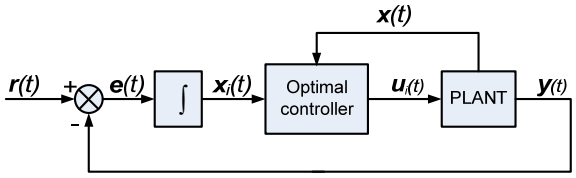

Fig. 3. Block diagram of the LQR with integral action

The integral control is introduced by considering the integral of the tracking error as an extra set of state variables (Jaen et al. (2006)). Thus, the plant model from (9) can be rewritten as:

$$\begin{cases} \dot{\mathbf{z}}(t) = \mathbf{A}_e\mathbf{z}(t) + \mathbf{B}_e\left[\mathbf{u}(t) + \mathbf{l}(t)\right] \\ \mathbf{y}(t) = \mathbf{C}_e\mathbf{z}(t) \end{cases}, \tag{10}$$

where,

$$\mathbf{z}(t) = \begin{bmatrix} i_{ds}(t) & i_{qs}(t) & i_e(t) & x_{ids}(t) & x_{iqs}(t) & x_{ie}(t) \end{bmatrix}^T,$$

$$\mathbf{A}_e = \begin{bmatrix} \mathbf{A} & \mathbf{O_3} \\ \mathbf{C} & \mathbf{I_3} \end{bmatrix}, \quad \mathbf{B}_e = \begin{bmatrix} \mathbf{B} \\ \mathbf{O_3} \end{bmatrix}, \quad \mathbf{C}_e = \begin{bmatrix} \mathbf{C} & \mathbf{O_3} \end{bmatrix},$$

x_{ids}, x_{iqs} and x_{ie} are the integral of the tracking currents error, $\mathbf{I_3}$ and $\mathbf{O_3}$ are the 3-dimensional identity and zero matrices.

The discrete form of (10) results as follows:

$$\begin{cases} \mathbf{z}(k+1) = \mathbf{\Phi}\mathbf{z}(k) + \mathbf{\Gamma}\left[\mathbf{u}(k) + \mathbf{l}(k)\right] \\ \mathbf{y}(k) = \mathbf{C}_e\mathbf{z}(k) \end{cases}, \tag{11}$$

where, $\mathbf{\Phi} = e^{\mathbf{A}_e T_{s1}}$, $\mathbf{\Gamma} = \int_0^{T_{s1}} e^{\mathbf{A}_e p}\mathbf{B}_e dp$ and T_{s1} denotes the sample time of currents control module.

If the infinite horizon LQR is employed, the following cost function must be minimized:

$$J(\mathbf{z}(k),\mathbf{u}(k)) = \sum_{k=0}^{\infty}\left(\mathbf{z}^T(k)\mathbf{Q}\mathbf{z}(k) + \mathbf{u}^T(k)\mathbf{R}\mathbf{u}(k)\right), \quad (12)$$

where $\mathbf{Q} = \mathbf{Q}^{\mathbf{T}} \geq 0$ and $\mathbf{R} = \mathbf{R}^{\mathbf{T}} > 0$ are constant state and input weight matrices.

Closed-loop optimal system must be stable, so the pair ($\mathbf{A}_e$, $\mathbf{B}_e$) must be stabilizable (and eventually controllable).

For finding the optimal feedback matrix, the discrete algebraic Riccati equation (DARE) must be solved (Arnold and Laub (1984), Lancaster and Rodman (1995)):

$$\Phi^T\left[\mathbf{P} - \mathbf{P}\Gamma\left(\Gamma^T\mathbf{P}\Gamma + \mathbf{R}\right)^{-1}\Gamma^T\mathbf{P}\right]\Phi + \mathbf{Q} - \mathbf{P} = \mathbf{0}. \quad (13)$$

The optimal control law results as:

$$\mathbf{u}(k) = -\left(\Gamma^T\mathbf{P}\Gamma + \mathbf{R}\right)^{-1}\Gamma^T\mathbf{P}\Phi\mathbf{z}(k) = \mathbf{K}\mathbf{z}(k). \quad (14)$$

Tuning linear quadratic controllers implies choosing the weight matrices **Q** and **R**. These matrices are usually chosen as diagonal matrices, so **Q** has n parameters and **R** has m parameters. For this case $n=6$ and $m=3$.

One possibility for the first choice of **Q** and **R** is according to Bryson's rule (Bryson and Ho (1975)).

3.2 Torque and Flux Estimator

This paper presents a method for estimating the torque from the estimated stator d and q axis flux linkages. From (2) estimated stator flux linkages in rotor reference frame can be expressed as follows:

$$\begin{aligned}\hat{\lambda}_{qs} &= \sum_{k=0}^{k_f-1}\left(v_{qs}(k) - \hat{r}_s(T)i_{qs}(k) - \omega_e(k)\hat{\lambda}_{ds}(k)\right)\\ \hat{\lambda}_{ds} &= \sum_{k=0}^{k_f-1}\left(v_{ds}(k) - \hat{r}_s(T)i_{ds}(k) + \omega_e(k)\hat{\lambda}_{qs}(k)\right)\end{aligned}. \quad (15)$$

In the above equation, the stator resistance is estimated as:

$$\hat{r}_s(T) = r(T_0)\cdot\left[1 + \alpha\left(T - T_0\right)\right], \quad (16)$$

where: T is the actual temperature, T_0 is the ambient temperature and α is the temperature coefficient of resistivity.

According to (6) the estimated torque results as follows:

$$\hat{T}_e = \frac{3P}{4}\left[\hat{\lambda}_d i_q - \hat{\lambda}_q i_d\right]. \quad (17)$$

3.3 Torque Deviation Controller

In order to keep the torque deviation at zero, the entire drive can be approximated with a first order transfer function. The time constant is given by the time response from currents controller and amplification gain varies around 1. For keeping the steady state error at zero, a LQR with integral action is designed. The augmented state space model of the plant with integral action is:

$$\begin{cases}\dot{\mathbf{z}}_t(t) = \mathbf{A}_t\mathbf{z}_t(t) + \mathbf{B}_t u_t(t)\\ y_t(t) = \mathbf{C}_t\mathbf{z}_t(t)\end{cases}, \quad (18)$$

where:

$$\mathbf{A}_t = \begin{bmatrix} -\frac{1}{T_{ds}} & 0\\ \frac{G_c}{T_{ds}} & 1\end{bmatrix},\quad \mathbf{B}_t = \begin{bmatrix}1\\0\end{bmatrix},\quad \mathbf{C}_t = \begin{bmatrix}\frac{G_c}{T_{ds}} & 0\end{bmatrix},$$

T_{ds} is the settling time for currents and G_c is amplification gain.

The discrete state-space form of (18) is:

$$\begin{cases}\mathbf{z}_t(k+1) = \mathbf{\Phi}_t\mathbf{z}_t(k) + \mathbf{\Gamma}_t u_t(k)\\ y_t(k) = \mathbf{C}_t\mathbf{z}(k)\end{cases}, \quad (19)$$

where, $\mathbf{\Phi}_t = e^{\mathbf{A}_t T_{s2}}$, $\mathbf{\Gamma}_t = \int_0^{T_{s2}} e^{\mathbf{A}_t p}\mathbf{B}_t dp$ and T_{s2} denotes the sample time of the torque control module.

The cost function given by (12) must be minimized to obtain the following optimal control law:

$$u_t(k) = -\left(\Gamma_t^T\mathbf{P}_t\Gamma_t + \mathbf{R}_t\right)^{-1}\Gamma_t^T\mathbf{P}_t\Phi_t\mathbf{z}_t(k) = \mathbf{K}_t\mathbf{z}_t(k), \quad (20)$$

where $\mathbf{P}_t$ is the solution of DARE:

$$\Phi_t^T\left[\mathbf{P}_t - \mathbf{P}_t\Gamma_t\left(\Gamma_t^T\mathbf{P}_t\Gamma_t + \mathbf{R}_t\right)^{-1}\Gamma_t^T\mathbf{P}_t\right]\Phi_t + \mathbf{Q}_t - \mathbf{P}_t = 0. \quad (21)$$

3.4 Current Referencer

The current referencer takes into account the torque versus speed characteristic presented in Fig. 4.

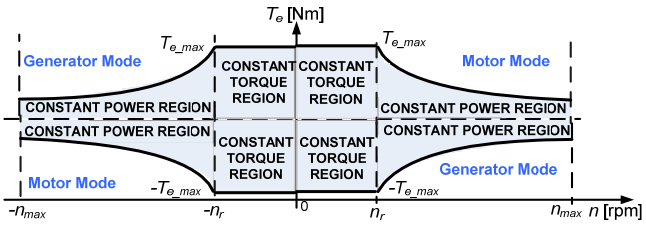

Fig. 4. Torque vs. Speed characteristic

For applications such as HEVs, the electric machine must be able to work in a wide speed range. Below the rated speed EESM can develop maximum torque and above rated speed, EESM can develop maximum power but the developed torque decreases with speed.

The zero d axis control (ZDAC) is not suitable for the EESM because it would lose the advantage of reluctance torque. Two strategies for generating the optimum reference currents can be implemented: maximum torque per ampere (MTPA) strategy for constant torque region and Field Weakening (FW) strategy for constant power region.

Below rated speed, because there are no voltage limitations, the current vector might be controlled to fully use the

reluctance torque to maximize the machine efficiency. In fact the torque per ampere ratio is maximized by controlling the current vector. From the voltage equations in the rotor reference frame, the steady-state phasor diagram of an EESM is shown in Fig. 5.

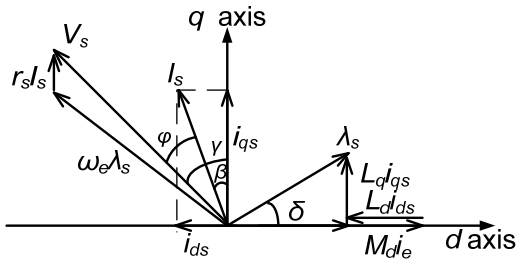

Fig. 5. EESM phasor diagram

In Fig. 5, β is the leading angles of the stator current vector, I_s is the stator current amplitude and V_s is the stator voltage amplitude. The d and q axis components of the stator current are given by:

$$\begin{aligned} i_{ds} &= -I_S \sin\beta \\ i_{qs} &= I_S \cos\beta \end{aligned} . \tag{22}$$

In this paper the following formula is proposed to generate the excitation reference current for the entire operation range:

$$i_e^* = \frac{T_e^* \cdot i_{e\_\max}}{T_{e\_\max}} . \tag{23}$$

Substituting (22) into (6) and taking into account (23) yields the expression for the torque in terms of the amplitude of the stator current as follows:

$$T_e = \frac{3P}{4} M_d i_e^* I_S \cos\beta + \frac{3P}{8}(L_q - L_d) I_S^2 \sin 2\beta . \tag{24}$$

The angle β must be controlled to obtain fast transient response and maximum torque with the smallest possible stator current amplitude. Setting the derivative of (24) with respect to β and imposing $\frac{dT_e}{d\beta} = 0$, the relationship between the stator current amplitude and the angle β is obtained as follows (Haque et al. (2003b)):

$$-\frac{3P}{4} M_d i_e^* I_S \sin\beta + \frac{3P}{4}(L_q - L_d) I_s^2 \left(\cos^2\beta - \sin^2\beta\right) = 0 . \tag{25}$$

From (22) and (25), the d-axis current component for MTPA strategy results:

$$i_{ds}^* = \frac{M_d i_e^*}{2(L_q - L_d)} - \sqrt{\frac{\left(M_d i_e^*\right)^2}{4(L_q - L_d)^2} - i_{qs}^{*2}} . \tag{26}$$

From (26) and (6), it is obtained:

$$i_{qs}^{*\,4} 36P^2 (L_q - L_d)^2 + i_{qs}^* 48P M_d i_e^* T_e^* - 64 T_e^{*2} = 0 . \tag{27}$$

The last equation has four roots, two real roots and two complex conjugate roots. From the two real roots, one is greater than the maximum admissible current. So, the q-axis current component from (27) is:

$$i_{qs}^* = \min_i \left\{ i_{qs\,i}^* \mid i_{qs\,i}^* \in \Re \right\}, i = \overline{1,4} . \tag{28}$$

If the rotor speed increases above the rated speed, the stator current and the voltage are limited by the power inverter and by the battery and the electric machine enters in FW region. The maximum stator current and voltage are expressed as:

$$I_S = \sqrt{i_{ds}^2 + i_{qs}^2} \le I_{sm} , \tag{29}$$

$$V_S = \sqrt{v_{ds}^2 + v_{qs}^2} \le V_{sm} , \tag{30}$$

where I_{sm} and V_{sm} are the available maximum stator current and voltage.

Substituting the voltage equations (4) into (30) and imposing $\frac{d\lambda_{qs}}{dt} = 0$ and $\frac{d\lambda_{ds}}{dt} = 0$ results:

$$V_S = \sqrt{\left(r_s i_{ds} - \omega_e L_q i_{qs}\right)^2 + \left(r_s i_{qs} + \omega_e L_d i_{ds} + \omega_e M_d i_e^*\right)^2} \le V_{sm} . \tag{31}$$

For rotor speed above rated, the stator resistance can be neglected because $r_s i_{ds} << \omega_e L_q i_{qs}$ and $r_s i_{qs} << \omega_e \left(L_d i_{ds} + M_d i_e^*\right)$. So, from (31) results i_{ds}* as follows:

$$i_{ds}^* = -\frac{M_d i_e^*}{L_d} + \frac{1}{L_d}\sqrt{\frac{V_{sm}^2}{\omega_e^2} - \left(L_q i_{qs}^*\right)^2} . \tag{32}$$

From (32) and (6), it is obtained:

$$\begin{aligned} &i_{qs}^{*4} 9P^2 \omega_e^2 L_q^2 (L_d - L_q)^2 + i_{qs}^{*2} [9P^2 \omega_e^2 L_q^2 \left(M_d i_e^*\right)^2 - 9V_{sm}^2 P^2 \cdot \\ &\cdot (L_d - L_q)^2] - i_{qs}^* 24P\omega_e^2 T_e^* L_d L_q M_d i_e^* + 16\omega_e^2 T_e^{*2} L_d^2 = 0. \end{aligned} \tag{33}$$

After solving (33), two complex conjugate roots and two real roots results. From the two real roots, the higher value should be chosen because otherwise i_{qs}* is greater than the maximum current amplitude I_{sm}. So, the q-axis current component from (33) is:

$$i_{qs}^* = \max_i \left\{ i_{qs\,i}^* \mid i_{qs\,i}^* \in \Re \right\}, i = \overline{1,4}. \tag{34}$$

The offline calculations are necessary to generate currents references. The selection between the two strategies is based on the modulation factor (M_f). The modulation factor is expressed as follows:

$$M_f = \frac{V_s}{V_{sm}} , \tag{35}$$

where $V_{sm} = \frac{V_{DC}}{\sqrt{3}}$ in the case when the space vector pulse width modulation is employed for controlling the power inverter.

4. SIMULATION RESULTS

In order to validate the model, a dynamic simulator is implemented in MATLAB/SIMULINK. The model of the plant is implemented using (1) through (8). The currents controller is implemented using (14). The torque and flux estimator is implemented using (15) through (17). For the torque deviation controller, (20) is used. The current referencer is implemented using data generated offline by solving (23) and (25) through (27) for the constant torque region and (23) and (32) through (34) for the constant power region. The entire control structure is designed to run in fixed-step using a dual-rate sampling approach, because the entire control structure takes into account a future implementation in an ECU. The current control algorithm is designed to run at 100 microseconds sample rate and the torque control is designed to run at 10 milliseconds sample rate.

Different simulation cases are presented to cover the entire operating range and to prove the advantages of the proposed control structure. In order to validate the model, a comparison with the data from a real test bench is performed. The test bench has two electric machines, one used to produce the torque load and the other is used as actuator machine under the test. The machines are connected back to back trough a mechanical shaft with torque and speed sensors. The structure of the test bench is presented in Fig.6.

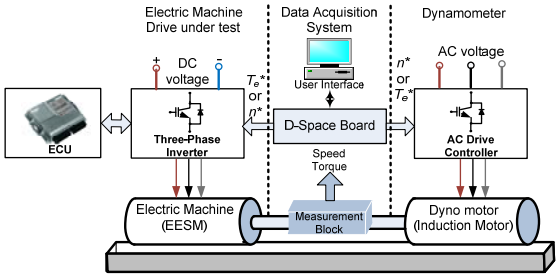

Fig. 6. Test bench structure

The EESM parameters are given by the test bench EESM specifications and are presented in Table A.1 in Appendix A. The optimal control matrices are given in Appendix B.

4.1 EESM Model Validation

First, the EESM model is validated against real electric machine. Fig. 7 shows the input signals, stator and excitation duty-cycles. After 3 seconds the duty-cycles increase.

The output signals of the model and of the real electric machine are presented in Fig. 8. As it can be seen in the Fig. 8.a the simulated and measured electromagnetic torque are considerably close, ensuring a small modeling error. In Fig 8.b it can be seen that the excitation current is also close to the measured current. The root-mean-square (RMS) currents for the stator are presented in Fig. 8.c. The error between RMS currents is greater at the beginning, but decrease in last 3 seconds, when the input signals increase.

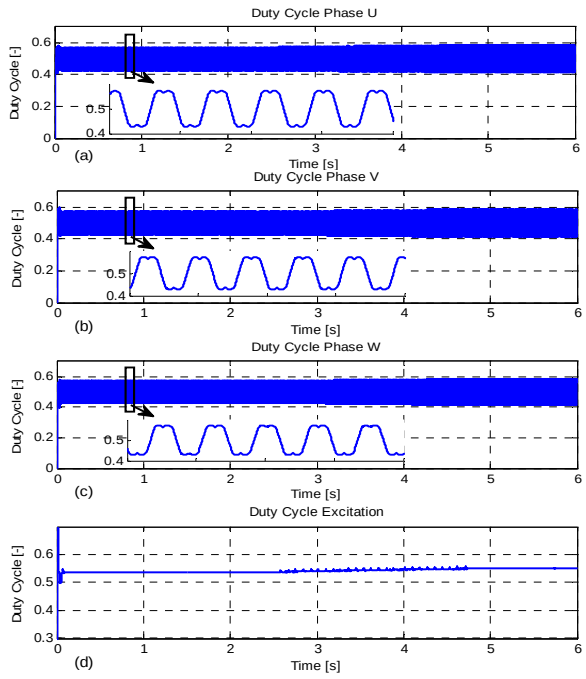

Fig. 7. Stator and excitation duty-cycles: (a) phase U duty-cycle, (b) phase V duty-cycle, (c) phase W duty-cycle, (d) excitation duty-cycle

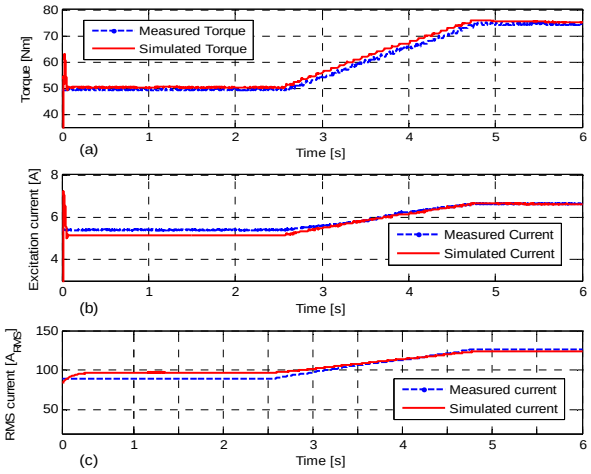

Fig. 8. Simulation responses compared with experimental measurements: (a) electromagnetic torque, (b) excitation current, (c) stator RMS current

4.2 Constant Torque Region Simulation

For this simulation case, a step reference torque with constant speed 1000 rpm is considered. The DC link voltage is set to 345 V. The simulation results are shown in Fig. 9 and 10. The EESM developed torque follows the reference. The torque sign can also be seen in the sign of the *q*-axis current. The *d*-axis current remain less than or equal with zero. The torque error is zero in steady state and has some spikes in transient state because the currents controller cannot respond instantly to the reference changes.

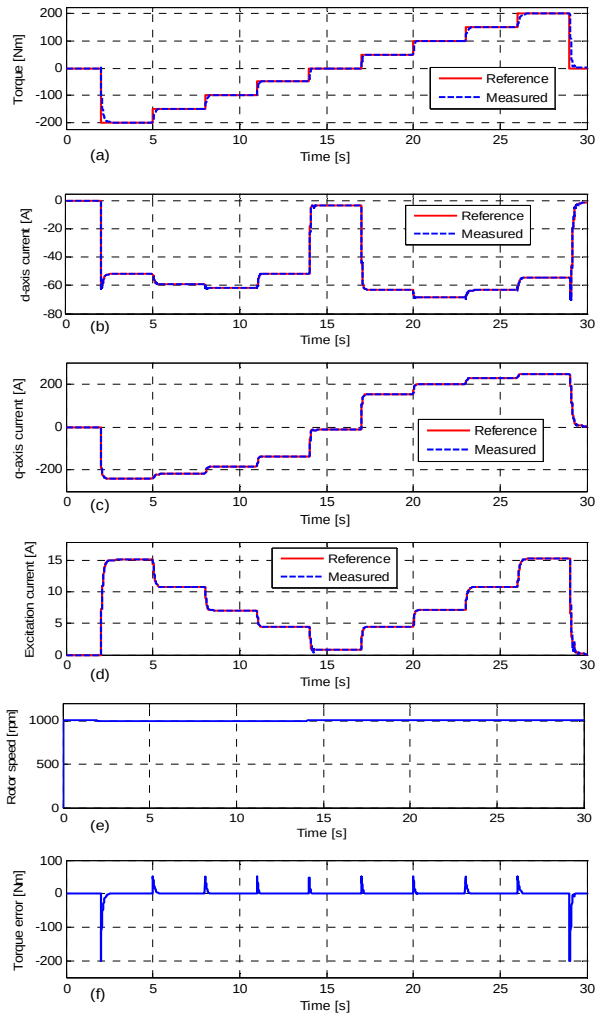

Fig. 9. EESM results (step torque, constant speed 1000 rpm): (a) reference and measured torque, (b) reference and measured *d*-axis current, (c) reference and measured *q*-axis current, (d) reference and measured excitation current (e) rotor speed, (f) torque error

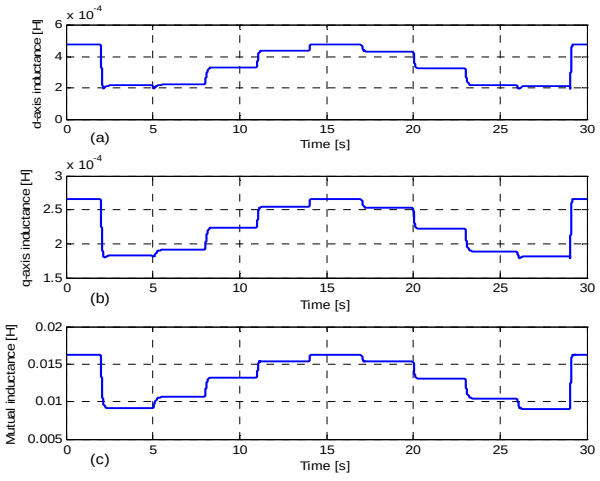

Fig. 10. EESM variation of parameters (step torque, constant speed 1000 rpm): (a) *d*-axis inductance, (b) *q*-axis inductance, (c) mutual inductance

The evolution of the EESM parameters can be seen in Fig. 10. Only the evolution of the *d*-axis inductance, *q*-axis inductances and mutual inductance are presented, because these parameters directly influence the electric machine torque. The influence of these variations is minimized by the torque deviation controller.

4.3 Constant Power Region Simulation

For the operation above rated speed, the results are shown in Fig. 11 and 12. In this case the EESM runs at constant speed of 4000 rpm.

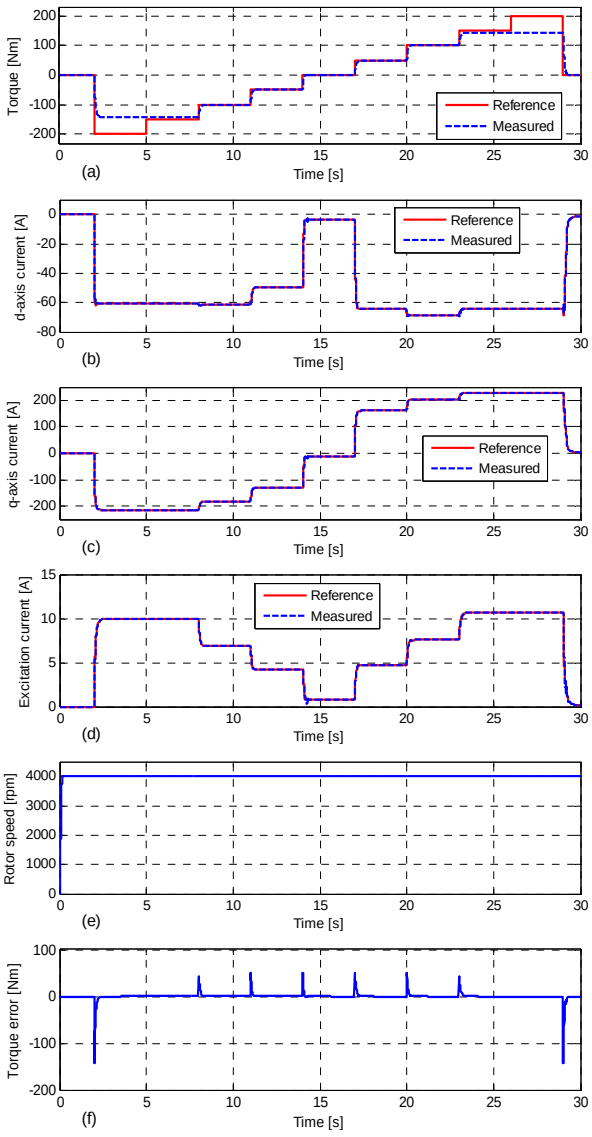

Fig. 11. EESM results (step torque, constant speed 4000 rpm): (a) reference and measured torque, (b) reference and measured *d*-axis current, (c) reference and measured *q*-axis current, (d) reference and measured excitation current (e) rotor speed, (f) torque error

The developed torque follows the reference and it is limited according to the maximum available torque at this speed. The stator *d*-axis current remains less than or equal to zero, and

the sign of the *q*-axis current follows the torque sign. The torque error is zero in the steady state, so the torque deviation controller does its job well.

The evolution of the EESM parameters in this case can be seen in Fig. 12.

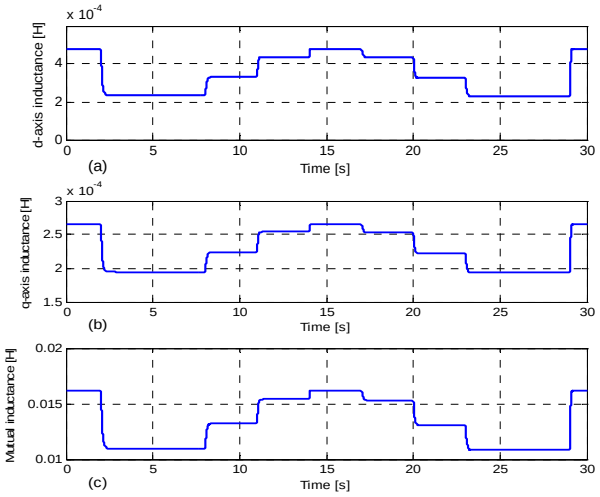

Fig. 12. EESM variation of parameters (step torque, constant speed 4000 rpm): (a) *d*-axis inductance, (b) *q*-axis inductance, (c) mutual inductance

4.4 Simulation with and without deviation control

Fig. 13 and 14 show the electric machine torque for the simulation with and without a deviation controller. When a deviation controller is used it can be seen that the time response is slightly higher but the steady-state error is zero. In case of simulation without a torque deviation controller the steady state error is greater than 15 Nm, which is a serious drawback in applications such as automotive propulsion.

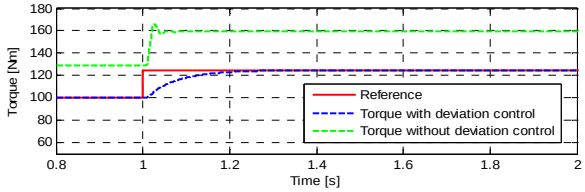

Fig. 13. EESM comparison between simulation with and without torque deviation control at 1000 rpm

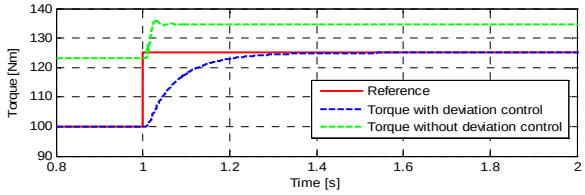

Fig. 14. EESM comparison between simulation with and without torque deviation control at 4000 rpm

4.5 Comparison between optimal and PID control

For comparison between the proposed control approach and classical PID approach, a PID controller for each current in the rotor reference frame (*d* and *q* axis currents and excitation current) is designed and tuned to have a fast response using Skogestad's method (O'Dwyer, 2009). For tuning the PID controllers the plant model for each current in the rotor reference frame was approximated with a first order transfer function.

Fig. 15 shows a comparison between optimal EESM control and classical PID control at 1000 rpm. As it can be seen, the optimal control strategy ensures minimum energy consumption in transient regime, while the PID control approach has a fast response.

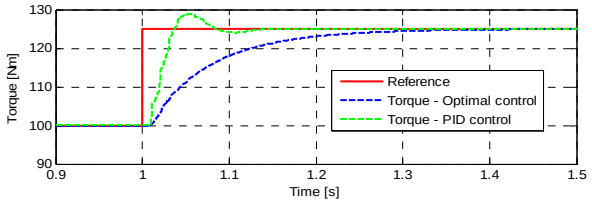

Fig. 15. EESM torque - comparison between optimal control and PID control at 1000 rpm

5. CONCLUSIONS

This paper presents a method that allows optimal torque control of EESMs. A complete mathematical model was presented and an optimal control architecture based on FOC scheme using a dual-rate sampling solution was designed, taking into account a future implementation on an ECU. The proposed control structure covers both the generator mode and the motor mode for traction EESMs. The presented control structure includes a torque estimator and an additional controller for minimizing the torque error. For the constant torque region, the MTPA strategy was used to obtain the currents references and, for the constant power region, FW strategy was used. These strategies are extensively studied in this paper.

The proposed control strategy also takes into account the variation of the machine parameters (stator inductances and mutual inductance between stator and rotor windings). The model was validated by comparing the obtained results with some data from a real test bench. Simulation and experimental results are comparable. The control structure shows good performance both in the constant torque region and in the constant power region. The results of the simulations illustrate a good behaviour of the proposed control scheme.

It also can be seen that the torque deviation controller significantly improves the results. The simulated results obtained with the proposed control strategy are compared with the ones obtained with the classical PID approach and the results show improved performances in term of power consumption in transient state.

REFERENCES

Aller, M., Bueno, A., and Paga, T. (2002). Power Systems Analysis Using Space-Vector Transformation, *IEEE Transactions on Power Systems*, Vol. 17, No. 4, pp. 957-965.

Anderson, B. D. O., Moore, J. B. (1989). Optimal Control: Linear Quadratic Methods, *Prentice-Hall International Inc.*

Arnold, W. F., and Laub, A. J. (1984). Generalized Eigenproblem Algorithms and Software for Algebraic Riccati Equations, *Proceedings of the IEEE*, Vol. 72, No. 12, pp. 1746-1754.

Benzi, F., Buja, G. S., and Felser, M. (2005). Communication Architectures for Electrical Drives, *IEEE Transactions on Industrial Informatics*, Vol. 1, No. 1, pp. 47-53.

Bryson, A. E., and Ho, Y. C. (1975). Applied Optimal Control: Optimization, Estimation, and control, *Taylor & Francis Group*, New York.

Casadei, D., Profumo, F., Serra, G., and Tani, A. (2002). FOC and DTC: Two Viable Schemes for Induction Motors Torque Control, *IEEE Transactions on Power Electronics*, Vol. 17, No. 5, pp. 779-787.

Haque, M. E., Zhong, L., and Rahman, M. F. (2003a). A Sensorless Initial Rotor Position Estimation Scheme for a Direct Torque Controlled Interior Permanent Magnet Synchronous Motor Drive, *IEEE Transactions on Power Electronics*, Vol. 18, No. 6, pp. 1376-1383.

Haque, M. E., Zhong, L. and Rahman, M. F. (2003b). Improved Trajectory Control for an Interior Permanent Synchronous Motor Drive with Extended Operating Limit, *Journal of Electrical & Electronics Engineering*, Australia, Vol. 22, pp. 49-57.

Hagstedt, D., Marquez, F., and Alakula, M. (2008). A comparison between PMSM, EMSM and SMSM in a BAS application, Proceedings of the *International Conference on Electrical Machines*, pp. 1-5.

Holtz, J. (1994). Pulsewidth Modulation for Electronic Power Conversion, *Proceedings of the IEEE*, Vol. 82, No. 8, pp. 1194-1214.

Houldsworth, J. A. and Grant, D. A. (1984). The Use of Harmonic Distortion to Increase the Output Voltage of a Three-Phase PWM Inverter, *IEEE Transactions on Industry Applications*, Vol. IA-20, No. 5, pp. 1224-1228.

Jaen, C., Pou, J., Pindado, R., Sala, V., and Zaragoza, J. (2006). A Linear-Quadratic Regulator with Integral Action Applied to PWM DC-DC Converters, *32nd IEEE Annual Conference on Industrial Electronics*, 2006, pp. 2280-2285.

Krause, P. C., Wasynczuk, O. and Sudhoff, S. D. (2002). Analysis of Electric Machinery and Drive Systems, 2nd Edition, *IEEE Series on Power Engineering*, *IEEE Press*.

Kwasinski, A., Krein, P. T., Chapman, P. L. (2003). Time Domain Comparison of Pulse-Width Modulation Schemes, *IEEE Power Electronics Letters*, Vol. 1, No. 3, pp. 64-68.

Lancaster, P., and Rodman, L. (1995). Algebraic Riccati Equations, *Oxford University Press*.

Malinowski, A., and Yu, H. (2011). Comparison of Embedded Systems Design for Industrial Applications, *IEEE Transactions on Industrial Informatics*, Vol. 7, No. 2, pp. 244-254.

Märgner, M., and Hackmann, W. (2010). Control challenges of an externally excited synchronous machine in an automotive traction drive application, *Emobility – Electrical Power Train*, pp. 1-6.

Monmasson, E., Idkhajine, L., Cirstea, M. N., Bahri, I., Tisan, A., and Naouar, M. W. (2011). FPGAs in Industrial Control Applications, *IEEE Transactions on Industrial Informatics*, Vol. 7, No. 2, pp. 224-243.

O'Dwyer, A. (2009). Handbook of PI and PID controller tuning rules, 3rd Edition, *Imperial College Press*.

Park, R. H. (1929). Two-Reaction Theory of Synchronous Machines – Generalized Method of Analysis, Part I, *AIEE Transactions*, Vol. 48, pp. 716-727.

Pillay, P., and Krishnan, R. (1988). Modeling of Permanent Magnet Motor Drives, *IEEE Transactions on Industrial Electronics*, Vol. 35, No. 4, pp. 537-541.

Salewski, F., and Kowalewski, S. (2008). Hardware/Software Design Considerations for Automotive Embedded Systems, *IEEE Transactions on Industrial Informatics*, Vol. 4, No. 3, pp. 156-163.

Takahashi, I., and Noguchi, T. (1988). A New Quick-Response and High-Efficiency Control Strategy of an Induction Motor, *IEEE Transactions on Industry Applications*, Vol. IA-22, No.5, pp. 820-827.

Tang, L., Zhong, L., Rahman, M., and Hu, Y. (2002). A Novel Direct torque Control for Interior Permanent Magnet Synchronous Machine Drive System with Low Ripple in Torque and Flux – A Speed Sensorless Approach, *IEEE Industry Applications Conference*, Vol. 1, pp. 104-111.

Vasudevan, M., and Arumugam, R. (2004). Different Viable Torque Controll Schemes of Induction Motor for Electric Propulsion System, *IEEE Industry Applications Conference*, Vol. 4, pp. 2728-2737.

Appendix A. PARAMETER VALUES

Table A.1 EESM parameters

Parameter	Value
Rated power (P_n)	60 kW
Rated torque (T_n)	225 Nm
Rated battery voltage (V_{dc})	345 V
Rated phase current (I_{sm})	350 A
Rated excitation current (i_{em})	18 A
Rated speed (n_r)	2500 rpm
Maximum speed (n_{max})	12000 rpm
Number of poles (P)	8
Nominal stator resistance (r_s)	0.00775 Ω
Nominal excitation resistance (r_e)	7.1 Ω
Nominal *d*-axis inductance (L_d)	0.0001488 H
Nominal *q*-axis inductance (L_q)	0.0002264 H
Nominal mutual inductance (M_d)	0.00906 H
Moment of inertia (J_m)	0.04 Kg·m^2
Viscous friction coefficient (B_m)	0.0001

Appendix B. CONTROL PARAMETERS

The optimal control matrices were obtained as:

$$\mathbf{K} = \begin{bmatrix} -0.1343 & 0 & -0.79 & -74.1679 & 0 & -9.0425 \\ 0 & -1.3675 & 0 & 0 & -135.27 & 0 \\ -2.9465 & 0 & -204.0545 & -546.09 & 0 & -1.31\cdot 10^{4} \end{bmatrix},$$

$$\mathbf{K}_{I=}\begin{bmatrix} -0.35 & -10 \end{bmatrix}.$$